

# Stability of electrostatic actuated membrane mirror devices

Peter Kurczynski, Harold M. Dyson, and Bernard Sadoulet

Membrane mirrors with transparent electrodes were fabricated for adaptive optics. These devices are capable of generating large, low-spatial-order deformations but exhibit instability for high-order deformations. A variational calculation of the electrostatic and mechanical energy of such membrane devices leads to criteria for stable operation. Simulations based upon this calculation are able to reproduce the observed behavior of fabricated devices and suggest suitable device parameters for improved performance with high-order deformations. © 2006 Optical Society of America

OCIS codes: 010.1080, 230.6120, 010.1290, 120.5060, 130.5990, 170.4460.

## 1. Introduction

Membrane deformable mirrors have been used as wavefront correctors for adaptive optics.<sup>1</sup> These devices consist of a grounded, conducting membrane suspended over an electrode array, which deforms the membrane via electrostatic actuation. Electrostatic pressure exerted on the membrane by charging underlying electrodes deforms the membrane. Microelectromechanical systems (MEMS) technology enabled the fabrication of inexpensive membrane mirrors that have been used in a wide variety of applications.<sup>2</sup> Recently, the need for wavefront deformations on the order of 10 μm for correction of aberrations in human vision, and greater degrees of freedom than are currently available for other adaptive optics applications, motivated the fabrication of devices made from low-stress silicon membranes.<sup>3</sup>

In widely available, single-electrode membrane devices, only the membrane tension provides an opposing, restoring force to deform the membrane in the opposite direction (due to the pull-in-only nature of electrostatic actuation). This characteristic is commonly considered a major drawback compared with segmented and continuous face-sheet deformable mirrors, where each segment has a restoring spring.

At the time of this research the authors were with the University of California at Berkeley, Berkeley, California 94720. H. M. Dyson is currently with Bell Laboratories, Lucent Technologies, Murray Hill, New Jersey 07974. For correspondence, please contact P. Kurczynski (pkurczynski@mac.com).

Received 16 March 2006; revised 5 July 2006; accepted 16 July 2006; posted 18 July 2006 (Doc. ID 69054).

0003-6935/06/328288-10\$15.00/0

© 2006 Optical Society of America

The devices considered here attempt to retain the simplicity of membranes while addressing the restoring force limitation by providing an additional, transparent electrode located above the membrane. In laboratory devices, transparent electrodes consisted of glass that was indium-tin-oxide-coated for electrical conductivity and visible light transmission. An electrode was inserted into a recessed cavity of each membrane chip and was fixed at 25–50 μm above the membrane. Charging the transparent electrode provided an electrostatic pressure that opposed the pressure exerted by the underlying electrode array and thereby allowed membrane deformation above and below the flat (unbiased) position. We address here the stability issues associated with these devices.

The devices were observed to be stable only within a limited range of operating voltages. Instability arose from increasing the electrostatic pressure on both sides of the membrane, as the electrode voltages were increased; instability manifested as membrane snapdown toward either electrode plane.

This paper presents an analysis of the stability of the membrane as a function of various device parameters and simulations of various device configurations to ascertain their stability and concludes with device parameters necessary to yield stable operation at large membrane deformation. The theory developed here agrees semiquantitatively with experimental results from laboratory experiments; this comparison will be discussed in a separate paper.<sup>3</sup>

## 2. Method

The static equilibrium of the membrane is analyzed by considering variations of the total electrostatic plus mechanical energy of the device. The first variation of the energy yields the equation of equilibrium, and the second variation of the energy is used to

analyze the stability of an arbitrary membrane deformation. The calculations of the total energy as well as the equation of equilibrium of the device are derived in Appendix A.

The analysis of stability, which leads to a matrix diagonalization problem, is covered in Section 3. To ascertain the stability of a given membrane deformation, the first and second variation of the total energy of the system are expressed as integrals over the membrane surface and computed using variational methods. Criteria for stability follow from demanding that the second variation of the energy be nonnegative, as discussed in Subsection 3.A. To complete the calculation, the energy functional is expressed in terms of the eigenfunctions of the membrane. In Subsection 3.B, this procedure leads to the diagonalization of a matrix and inspection of its eigenvalues as a method for ascertaining the stability of arbitrary membrane deformations.

Implementation of the matrix diagonalization method to simulate device performance is covered in Section 4. Inspection of the eigenvalues of the diagonalized matrix is used to determine the stability of input membrane configurations. Simulations are used to explore the stability of various device geometries and to guide the design of future devices intended for large membrane deformation. Section 5 includes results of these simulations and comparison with data from laboratory devices.

### 3. Stability Analysis of the Membrane Device

#### A. Second Variation of the Energy Function

A membrane with tension  $T$  suspended a distance  $d_A$  from an electrode array and a distance  $d_T$  from a transparent electrode is schematically illustrated in cross section in Fig. 1. The membrane is circular with radius  $a$ , not shown in Fig. 1. The entire electrode array is charged to a uniform voltage  $V_A$ ; the transparent electrode is charged to a voltage  $V_T$ . Voltages are defined relative to the membrane, which is not necessarily at ground. The membrane shape is described by a deformation function  $\xi$  of two coordinates in the plane of the membrane. The positive direction of deformation is defined as toward the electrode array, which is the bottom electrode in the figure. Figure 1 illustrates a deformation toward the transparent electrode to emphasize that such deformations are physically realizable with the device.

The first variation of the combined electrostatic and mechanical energy of such a system,  $\delta U$ , is derived in Appendix A and is given by an integral over the membrane surface  $S$  in two dimensions:

$$\delta U = \int \left[ -T \nabla^2 \xi - \frac{1}{2} \epsilon_0 \frac{V_A^2}{(d_A - \xi)^2} + \frac{1}{2} \epsilon_0 \frac{V_T^2}{(d_T + \xi)^2} \right] \delta \xi dS, \quad (1)$$

where  $\epsilon_0$  is the permittivity of free space. From this expression, the second variation of the energy can be

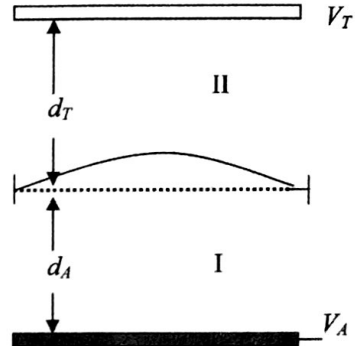


Fig. 1. Schematic diagram of a membrane mirror device. The membrane, solid curve, is located between the top transparent electrode located at a distance  $d_T$  and the bottom actuating electrode located at a distance  $d_A$ . The membrane experiences deformations relative to the flat position (dotted line) in response to electric fields in regions I and II. Voltages  $V_A$  and  $V_T$  refer to the relative voltage between the respective electrode plane and the membrane, which may be at ground or at some nonzero voltage.

found by differentiating Eq. (1) and disregarding terms of order  $\delta^2 \xi$  yields

$$\delta^2 U = \int \left[ -T \nabla^2(\delta \xi) - \frac{\epsilon_0 V_A^2}{(d_A - \xi)^3} \delta \xi - \frac{\epsilon_0 V_T^2}{(d_T + \xi)^3} \delta \xi \right] \delta \xi dS. \quad (2)$$

The second and third terms of the integrand, involving electrostatic quantities, can be combined into a single weight function:

$$\mathcal{F}(\xi) \equiv \frac{\epsilon_0 V_A^2}{(d_A - \xi)^3} + \frac{\epsilon_0 V_T^2}{(d_T + \xi)^3}. \quad (3)$$

Thus the second variation of the energy may be regarded as being composed of a tension term  $\delta^2 U_T$  and an electrostatic term  $\delta^2 U_E$  as follows:

$$\begin{aligned} \delta^2 U &= - \int T \nabla^2(\delta \xi) \delta \xi dS - \int \mathcal{F}(\xi) (\delta \xi)^2 dS \\ &\equiv \delta^2 U_T + \delta^2 U_E. \end{aligned} \quad (4)$$

This expression can be simplified by expressing the variation of the membrane deformation  $\delta \xi$  as a series expansion into eigenfunctions of the membrane  $\zeta_{vn}$ , which are discussed in Appendix B. Defining the expansion coefficients as  $b^{vn}$ , the variation of the deformation is expressed as

$$\delta \xi = \sum_{v,n} b^{vn} \zeta_{vn}. \quad (5)$$

The double summation is over the eigenfunctions of the membrane, indexed by  $v$  and  $n$ . In practice, a finite set is used to approximate the infinite sum, where the number of eigenfunctions used for each

index is defined as  $V$  and  $N$ , respectively. Taking the complex conjugate of Eq. (5), where  $\bar{b}^{vn}$  denotes the complex conjugate of  $b^{vn}$ , etc., and using the fact that  $\delta\xi$  is real, yields

$$\delta\xi = \sum_{v,n} \bar{b}^{vn} \zeta_{vn}. \quad (6)$$

Inserting the above expansions into the expression for  $\delta^2U_T$  yields

$$\delta^2U_T = \int \left[ -T\nabla^2 \left( \sum_{v,n} b^{vn} \zeta_{vn} \right) \sum_{v',n'} \bar{b}^{v'n'} \bar{\zeta}_{v'n'} \right] dS. \quad (7)$$

Equation (7) can be further simplified using the eigenvalue equation for the basis functions  $\zeta_{vn}$ , which is discussed in Appendix B:

$$\nabla^2 \zeta_{vn} = -\left(\frac{x_{vn}}{a}\right)^2 \zeta_{vn}. \quad (8)$$

This expression equates the Laplacian of the eigenfunction to the product of the eigenfunction and its eigenvalue, which includes the membrane radius  $a$  and the  $n$ th zero of Bessel function  $v$ ,  $x_{vn}$  (see Appendix B for details).

Using Eq. (8) to evaluate the Laplacian in Eq. (7) leads to

$$\delta^2U_T = \int \left[ T \left( \sum_{v,n} b^{vn} \left( \frac{x_{vn}}{a} \right)^2 \zeta_{vn} \right) \sum_{v',n'} \bar{b}^{v'n'} \bar{\zeta}_{v'n'} \right] dS, \quad (9)$$

$$\delta^2U_T = T \sum_{v,v',n,n'} \left( \frac{x_{vn}}{a} \right)^2 b^{vn} \bar{b}^{v'n'} \int \zeta_{vn} \bar{\zeta}_{v'n'} dS. \quad (10)$$

Finally, orthonormality of the basis functions  $\zeta_{vn}$ , given in Appendix B by Eq. (B4), is used to compute the integral in Eq. (10):

$$\delta^2U_T = T \sum_{v,v',n,n'} \left( \frac{x_{vn}}{a} \right)^2 b^{vn} \bar{b}^{v'n'} \delta_{vv'} \delta_{nn'}, \quad (11)$$

where each  $\delta$  denotes a Kronecker delta; these factors simplify the summation, which yields

$$\delta^2U_T = T \sum_{v,n} \left( \frac{x_{vn}}{a} \right)^2 b^{vn} \bar{b}^{vn}. \quad (12)$$

The electrostatic term  $\delta^2U_E$  in Eq. (4) can also be simplified using the expansions in terms of the membrane eigenfunctions given by Eqs. (5) and (6):

$$\delta^2U_E = - \int \mathcal{F}(\xi) \sum_{v,n} b^{vn} \zeta_{vn} \sum_{v',n'} \bar{b}^{v'n'} \bar{\zeta}_{v'n'} dS. \quad (13)$$

The components of the second variation of the energy, given by Eqs. (12) and (13), can be combined and used

to investigate the stability behavior of a membrane device under a variety of conditions and device parameters. A stable device configuration has  $\delta^2U > 0$ . For small deformations, an analytic criterion for stability can be derived; however, stability analysis of large deformations requires a numerical computation, which is discussed in Subsection 3.B.

### B. Stability of the Membrane: Diagonalization of the Stability Matrix

In this subsection, we demonstrate that for arbitrary deformations of the membrane,  $\delta^2U$  can be reduced to a matrix expression of the form

$$\delta^2U = \tilde{b}^\dagger \Omega \tilde{b}, \quad (14)$$

where the vector  $\tilde{b}$  is constructed from the expansion coefficients  $b^{vn}$  of the membrane deformation, the dagger denotes an adjoint, and the matrix  $\Omega$ , derived below, includes all device-dependent parameters. A necessary and sufficient condition for stability is that  $\Omega$  be positive definite. Thus, diagonalization of this matrix and inspection of its eigenvalues leads to a criterion for stability of the membrane.

For arbitrary deformations of the membrane, the function  $\mathcal{F}(\xi)$  cannot be moved outside the integral in Eq. (13). However, the double summations in Eq. (13) can be rewritten as single summations by defining new indices  $j$  and  $j'$ , where each value of the new index corresponds to a unique combination of  $v$  and  $n$ . For example, in simulations discussed in Section 4, eigenfunctions were encoded according to  $j = 9v + n - 1$ ; these simulations included 53 eigenfunctions with the lowest 5 values of  $v$  and the lowest 9 values of  $n$ . Writing Eq. (13) in terms of a single summation yields

$$\delta^2U_E = - \int \mathcal{F}(\xi) \sum_j b^j \zeta_j \sum_{j'} \bar{b}^{j'} \bar{\zeta}_{j'} dS. \quad (15)$$

Moving the summations and the expansion coefficients  $b^j$  and  $\bar{b}^{j'}$  outside the integral and defining the integral as a matrix element yield

$$\delta^2U_E = - \sum_{j,j'} b^j \bar{b}^{j'} A_{jj'}, \quad (16)$$

where the matrix element is defined as

$$A_{jj'} = \int \mathcal{F}(\xi) \zeta_j \bar{\zeta}_{j'} dS. \quad (17)$$

Similarly, rewriting the summation in Eq. (12) in terms of the new indices  $j$  and  $j'$  yields

$$\delta^2U_T = T \sum_j \left( \frac{x_j}{a} \right)^2 b^j \bar{b}^j. \quad (18)$$

Anticipating combining this expression with the corresponding expression for  $\delta^2U_E$ , Eq. (18) can be

written in terms of a double sum over  $j$  and  $j'$  as

$$\delta^2 U_T = \sum_{j,j'} T \left( \frac{x_j}{a} \right)^2 b^j \bar{b}^{j'} \delta_{jj'}, \quad (19)$$

where  $\delta_{jj'}$  is a Kronecker delta.

The two components of  $\delta^2 U$  can be combined to give

$$\delta^2 U = \delta^2 U_T + \delta^2 U_E = T \sum_{j,j'} \left( \frac{x_j}{a} \right)^2 b^j \bar{b}^{j'} \delta_{jj'} - \sum_{j,j'} b^j \bar{b}^{j'} A_{jj'}, \quad (20)$$

$$\delta^2 U = \sum_{j,j'} \left[ T \left( \frac{x_j}{a} \right)^2 \delta_{jj'} - A_{jj'} \right] b^j \bar{b}^{j'}. \quad (21)$$

The quantity in square brackets can be represented as a Hermitian matrix:

$$\Omega \equiv \begin{bmatrix} T \left( \frac{x_1}{a} \right)^2 - A_{11} & \cdots & -A_{1M} \\ \vdots & \ddots & \vdots \\ -A_{M1} & \cdots & T \left( \frac{x_M}{a} \right)^2 - A_{MM} \end{bmatrix}. \quad (22)$$

The dimension  $M$  of this matrix spans all of the  $V \times N$  basis functions used in the expansions of Eqs. (12) and (13). The matrix  $\Omega$  can be diagonalized by a similarity transformation, whereby the resulting diagonal entries of the matrix are its eigenvalues  $\lambda_j$ . Operating on Eq. (21) with this similarity transformation leads to an equivalent expression for  $\delta^2 U$  as the sum of the product of these eigenvalues with the norms of the expansion coefficients  $b^j$ :

$$\delta^2 U = \sum_{j=1}^M \lambda_j \|b^j\|^2. \quad (23)$$

Requiring stability of the equilibrium imposes the condition  $\delta^2 U > 0$  for an arbitrary deformation, which is characterized by the expansion coefficients  $b^j$ . Because the norms of the expansion coefficients are nonnegative, a necessary condition for stability is therefore that all of the eigenvalues  $\lambda_j$  be nonnegative. If even a single eigenvalue is negative, then a particular deformation corresponding to that eigenmode will lead to  $\delta^2 U < 0$ ; the stability criterion will have been violated for (at least that one) deformation, and therefore the condition for arbitrary deformations will have also been violated. We observe that as the index is increased, the eigenvalues increase, and therefore we focus our attention on the lowest-order eigenvalues.

In the simulations presented below, analysis of the eigenvalues  $\lambda_j$  was used to determine the stability characteristics of membrane devices. If the lowest eigenvalue was negative, then the simulated device configuration was deemed unstable. When considering a range of device parameters, such as operating

voltages, the range over which the lowest eigenvalue remains nonnegative determined the range of stable operation of the device.

#### 4. Device Simulation

A procedure for diagonalizing the stability matrix outlined in Subsection 3.B was implemented in software to enable the investigation of various device parameters for their stability characteristics. The simulations began with an input membrane deformation  $\xi$ , expressed as a series expansion of eigenfunctions of the membrane. The required electrode voltages were computed in a self-consistent manner, as discussed below. From these voltages, the matrix elements  $A_{jj'}$ , defined in Eq. (17), were computed by summing over discrete electrode array elements, as discussed below.

For comparison and validation of the code, matrix elements were also computed using the integral expression given by Eq. (17). For small deformation amplitudes and electrode voltages, these methods of computation gave similar results. The advantage of the numerical computation is its applicability to both small and large deformations, both of which are encountered in laboratory devices.

The stability matrix  $\Omega$  given by Eq. (22) was computed and diagonalized to yield a set of eigenvalues and eigenvectors. The eigenvalues were used to determine stability; negative eigenvalues for a given simulation indicated an unstable device configuration. Simulations were run with varying gap distances, membrane tension, and electrode voltages to identify the parameter space for stable operation and determine optimum parameters for device stability.

A self-consistent simulation of the device performance requires that the voltages  $V_A$  and  $V_T$  be consistent with the actual deformation of the membrane, as given by Eq. (A12) in Appendix A. Furthermore, the analysis so far has considered the electrode array to be energized to a single, uniform voltage  $V_A$ , whereas in practice each electrode of the array will have a unique voltage applied to it. For a given membrane deformation function  $\xi$ , the required electrode voltages may be obtained from Eq. (A12) by solving for  $V_A$ . Then the membrane deformation function is evaluated at the positions of the electrode centers, i.e.,  $\xi_k = \xi(\mathbf{r}_k)$ , where  $\mathbf{r}_k$  denotes the position of electrode  $k$  on the electrode plane. Locations of electrode elements are chosen to model actual devices that were fabricated and tested in the laboratory. Thus the discrete electrode voltages are given by

$$V_k^2 = \frac{2(d_A - \xi_k)^2}{\epsilon_0} \left[ \frac{\epsilon_0 V_T^2}{(d_T + \xi_k)^2} - T \nabla^2 \xi_k \right]. \quad (24)$$

The quantity in the brackets of Eq. (24) must be nonnegative for physically realizable membrane deformations. This restriction places a lower limit on the transparent electrode voltage  $V_T$ . Provided that this lower limit is satisfied, the membrane deformation and voltages can be made self-consistent.

The corresponding electrostatic weight function, the discretization of Eq. (3), is given by

$$\mathcal{F}(\mathbf{r}_k) = \epsilon_0 \frac{V_k^2}{(d_A - \xi_k)^3} + \epsilon_0 \frac{V_T^2}{(d_T + \xi_k)^3}. \quad (25)$$

The matrix element, given by Eq. (17), is computed by approximating the surface integral as a sum over the membrane surface:

$$A_{jj'} = \sum_k \mathcal{F}(\mathbf{r}_k) \zeta_j(\mathbf{r}_k) \zeta_{j'}(\mathbf{r}_k) \Delta s_k. \quad (26)$$

The sum is over patches of the membrane surface that correspond to electrodes of the underlying array, as well as equally sized patches that extend from the periphery of the array to the outer edge of the membrane. These patches completely tile the membrane surface. In calculations below, the sum consisted of 2916 terms, corresponding to a  $54 \times 54$  grid.

## 5. Results of Simulation

### A. Range of Stable Device Operation

Simulations of devices with a transparent electrode indicate that stable operation of the devices depends upon judicious choice of membrane-electrode gap distances and operating voltages. In a device with a transparent electrode, the membrane is pulled from both sides by the opposing electrodes. This competition of forces leads to instability. In general, larger gap distance devices can operate over a wider range of deformations than smaller gap distance devices. However, large deformations require high transparent electrode voltages, which limit the domain of stability for a given device.

Increasing the membrane tension (stress  $\times$  thickness) also increases stability; however, highly tensile membranes require larger voltages to generate a given deformation. The simulations discussed below use a membrane tension of 3 N/m, corresponding to 3 MPa stress and 1  $\mu\text{m}$  thickness membranes, similar to devices that have been fabricated and reported previously.

Figure 2 illustrates the eigenvalue variation as a function of peak deformation for various device configurations. Positive eigenvalues correspond to stable device configurations; negative eigenvalues correspond to unstable device configurations. These data were obtained using a  $J_0$  Bessel function input and the computational procedure described above. The input membrane shape for these simulations was approximately parabolic, eigenfunction  $j = 0$ , see Fig. 6 in Appendix B, and therefore of low spatial order. Higher-spatial-order deformations are considered in Subsection 5.B. The upper dashed curve of Fig. 2 illustrates a simulated device with a 75  $\mu\text{m}$  membrane-electrode array and 75  $\mu\text{m}$  membrane-transparent electrode gap distances. The corresponding electrode array voltages were computed in a self-consistent manner

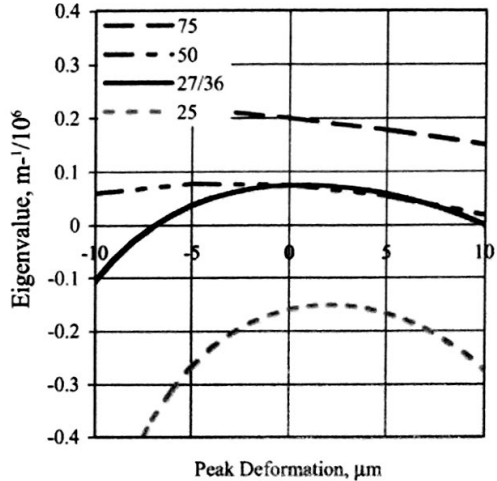


Fig. 2. (Color online) Lowest stability matrix eigenvalue versus peak deformation for several devices with different gap distances. Peak deformations that can be achieved with stable device operation are indicated by positive eigenvalues. Large gap distance devices can achieve a broader range of peak deformations than small gap distance devices. Deformation is the lowest-order membrane function,  $j = 0$ . Dashed curves correspond to simulated devices with membrane-transparent electrode distances (equal to membrane-electrode array distances): 75  $\mu\text{m}$  (top), 50  $\mu\text{m}$  (middle), and 25  $\mu\text{m}$  (bottom). The left-right asymmetry of the data is a consequence of differing geometries of the two electrode surfaces. The middle solid curve illustrates the model of an actual device, which was tested in the laboratory, with asymmetrical 27/36  $\mu\text{m}$  gap distances.

as described in Section 4. This device is stable over a broad range of deformations; however, the range of deformation toward the transparent electrode, corresponding to negative deformations in Fig. 2, is limited to 5  $\mu\text{m}$  by the transparent electrode potential, which was 50 V. Increasing the operating voltage allows greater negative deformations, but diminishes the overall region of stability.

Devices with smaller gap distances, illustrated in Fig. 2, have reduced regions of stability. The middle dashed-dotted curve corresponds to 50  $\mu\text{m}$  symmetric gap distances and 40 V transparent electrode potential; the lower dashed curve corresponds to 25  $\mu\text{m}$  gap distances and 20 V transparent electrode potential.

The middle solid curve of Fig. 2 illustrates the simulation of a device fabricated in the laboratory. This device has a 27  $\mu\text{m}$  transparent electrode-membrane gap distance and a 36  $\mu\text{m}$  membrane-electrode array gap distance, and the simulation indicates stable operation from  $-7$  to  $10$   $\mu\text{m}$ . Laboratory experiments with this device were able to demonstrate  $\pm 10$   $\mu\text{m}$  deformation, indicating broad agreement of the simulation with the actual device.<sup>3</sup>

Simulations indicate that devices with large gap distances can operate with large electrode voltages in a stable manner. Large electrode voltages are desirable because they increase the overall range of achievable deformations at all spatial orders; however, devices that operate in excess of 100 V may be more difficult to fabricate and/or operate, particularly if on-chip electronics are desired.

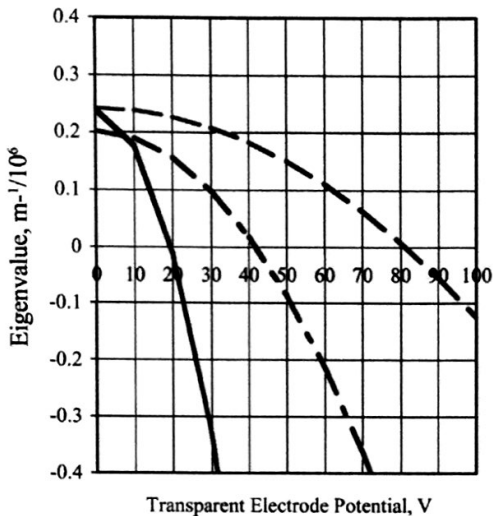


Fig. 3. (Color online) Lowest stability matrix eigenvalue versus transparent electrode potential for several devices with different gap distances. The voltages for stable device operation are indicated by positive eigenvalues. Large gap distance devices are stable over a wider range of electrode voltages than small gap distance devices. Dashed curves correspond to simulated devices with membrane-transparent electrode distances (equal to membrane-electrode array distances): 75  $\mu\text{m}$ , top curve (dashed), and 50  $\mu\text{m}$ , middle curve (dotted-dashed). Solid lower curve illustrates the model of an actual device, which was tested in the laboratory, with asymmetrical 27/36  $\mu\text{m}$  gap distances.

Figure 3 illustrates the stability matrix eigenvalues versus transparent electrode potential for a set of devices and membrane configurations. The upper dashed curve of Fig. 3 corresponds to a 75  $\mu\text{m}$  symmetric gap distance device, producing a membrane deformation of 10  $\mu\text{m}$  peak deformation; this configuration is stable from 0 to 80 V. The middle dashed-dotted curve illustrates 10  $\mu\text{m}$  peak deformation produced by a device with 50  $\mu\text{m}$  symmetric gap distances; this device configuration is stable from 0 to 40 V.

The solid curve of Fig. 3 illustrates a simulation of a device with 27/36  $\mu\text{m}$  gap distances corresponding to a device that was fabricated and tested in the laboratory. This simulated device is stable at transparent electrode potentials up to 20 V. The actual device tested in the laboratory was found to become unstable with transparent electrode potentials in excess of approximately 17 V.<sup>3</sup> We interpret this general agreement between the simulation and the experimental device as a validation of the method of simulation. The residual discrepancy between computed and observed voltage limits may have arisen due to a slight misalignment of the electrode array and membrane of the laboratory device.

#### B. Maximum Stable Deformation

In general, electrostatic actuated MEMS devices become unstable and experience snapdown when the actuation distance is one third the gap distance between undeformed electrodes. This result can be derived analytically for discrete, segmented electrode actuators.

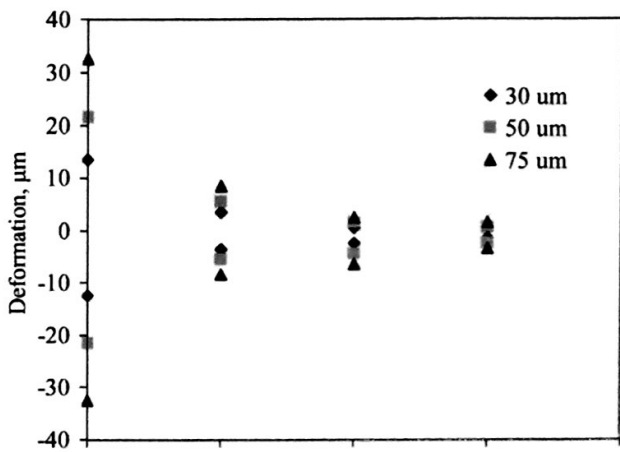


Fig. 4. (Color online) Maximum, stable peak deformation for the lowest eigenmodes of membrane devices for several different membrane-electrode gap distances. Positive deformations are toward the transparent electrode; negative deformations are toward the electrode array. These data quantify the capability of membrane devices to generate deformations at each spatial order.

Simulations indicate that a more complex relationship pertains for membrane devices. Membrane devices can achieve stable deformations larger than the one-third gap limit for the lowest eigenmode; however, they are limited to less than the one-third gap limit for higher-spatial-order deformations. Higher-order modes require higher voltages that lead to instability.

Figure 4 quantifies the extent of achievable membrane deformation at various spatial orders. These data illustrate the maximum peak deformation of several membrane devices as a function of eigenmode number. The first four eigenmodes were studied in simulated devices with 30, 50, and 75  $\mu\text{m}$  membrane-electrode gap distances. Membrane radius was 7.5 mm, tension was 3 N/m (3 MPa stress; 1  $\mu\text{m}$  thickness). Each eigenmode was a Bessel function of the radial coordinate, as illustrated in Fig. 5(a) for the  $j = 2$  eigenmode. The potential distributions required to produce the deformations were also computed, as illustrated in Fig. 5(b) for the  $j = 2$  eigenmode.

Device stability depends upon the transparent electrode potential, as discussed above. The data for Fig. 4 were obtained by selecting the minimum transparent electrode voltage that would allow the device to produce the required deformation. This voltage was selected by an iterative procedure: A low initial trial voltage was used, and the corresponding electrode array voltage distribution (required to generate the desired membrane deformation) was computed. In general, this distribution consisted of complex-valued quantities. Imaginary voltages were unphysical and indicated that the transparent electrode voltage needed to be increased for the device to be capable of producing the required deformation. This voltage was increased incrementally until the corresponding electrode array voltage distribution was entirely real.

For low-spatial-order deformations, the membrane can deform to greater than the one-third gap distance limit normally associated with MEMS devices, as

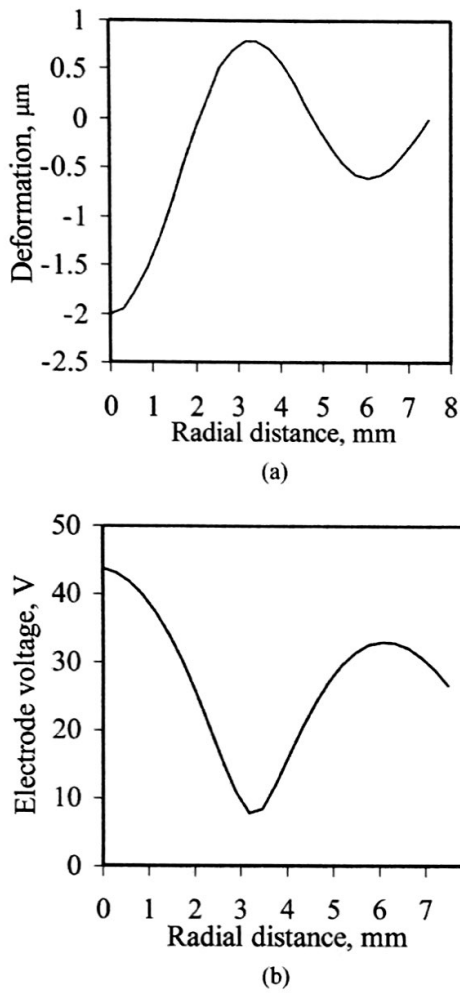


Fig. 5. (a) Membrane deformation corresponding to  $j = 2$  eigenmode. Largest magnitude deformation is toward the electrode array (negative value on vertical axis). (b) Voltage distribution on the array necessary to produce the deformation from (a), with a device having 30  $\mu\text{m}$  gap distances and 25 V transparent electrode potential.

illustrated in Table 1. This table illustrates the maximum amplitude deformation obtained for single-electrode plane devices based on the eigenvalue analysis. Amplitude here is defined as the maximum zero-to-peak (or trough) distance, which for the Bessel function is measured at  $r = 0$ . The first column is the membrane-electrode array gap distance for the simulated device. The second column indicates the peak deformation at which instability occurs based

Table 2. Maximum Deformation for First-Order ( $j = 1$ ) Eigenmode in Several Devices

Device Gap Distance ( $\mu\text{m}$ )	Maximum Deformation ( $\mu\text{m}$ )	One-Third Gap Distance ( $\mu\text{m}$ )	% One-Third Gap Attained	Maximum Array Potential (V)
30	3.5	10.0	35	33
50	5.5	16.7	33	71
75	8.5	25.0	34	110

upon the stability matrix computation. The third column indicates the one-third gap distance for the device. The last column indicates the peak deformation as a percentage of the one-third gap distance.

Various membrane-electrode gap distances were simulated. The membrane tension was 3 N/m and the membrane radius was 7.5 mm. The input membrane shape was the lowest-order membrane eigenfunction  $j = 0$ . The resulting peak deformation was toward the electrode plane; the value of the peak deformation was approximately 130% one-third gap distance for all simulations.

The membrane cannot generate higher-spatial-order deformations as effectively as lower-spatial-order deformations, as illustrated in Table 2. This table illustrates the maximum amplitude deformation obtained for transparent electrode plane devices that are capable of deformation toward either electrode plane. Device parameters are the same as the data in Table 1; however, the membrane shape was the membrane eigenfunction  $j = 1$ . The radial component of this eigenfunction has a single node midway between the membrane center and the edge, and no azimuthal dependence. The first column indicates the membrane-electrode gap distance. The second column indicates the maximum stable deformation (toward transparent electrode), from stability matrix computation. The third column indicates the one-third gap distance, and the fourth column indicates the percentage of the one-third gap value achieved by the maximum deformation. The last column indicates the peak voltage on the array necessary to produce the deformation. The maximum amplitude of stable deformation obtained with this higher-spatial-order eigenfunction is 30%–35% one-third gap distance. Further simulations with  $j = 2$  and  $j = 3$  eigenfunctions, corresponding to two and three radial nodes and no azimuthal dependence, support this conclusion, as illustrated in Fig. 4.

## 6. Conclusion

Our simulations identify membrane stability as the principal engineering challenge to producing high-performance membrane mirrors with transparent electrodes. Low-stress membranes that utilize a transparent electrode will enable large-amplitude, high-spatial-order deformations suitable for wavefront correction in adaptive optics. The amplitude as a function of spatial order (i.e., spatial-frequency response) is not limited by bending stress, as has

Table 1. Maximum Deformation for Lowest-Order ( $j = 0$ ) Eigenmode in Several Devices

Device Gap Distance ( $\mu\text{m}$ )	Maximum Deformation ( $\mu\text{m}$ )	One-Third Gap Distance ( $\mu\text{m}$ )	% One-Third Gap Attained
30	13.5	10.0	135
50	21.5	16.7	129
75	32.5	25	130

been previously supposed; instead, it is limited by the requirement of kinematic stability of the membrane. For judicious choice of device parameters, the stability criterion does not restrict membranes from generating the deformations required for adaptive optics applications. Devices with larger gap distances than the current devices would be more stable. With low-stress membranes, such devices would still operate at lower voltage than existing membrane mirrors and achieve greater deformation at all spatial orders than has been realized to date.

The requirement of kinematic stability constrains the membrane-electrode gap distances and operating voltages for a transparent electrode membrane device. Devices with larger gap distances are more stable, but they require larger operating voltages to achieve a given deformation. Increasing the operating voltages also leads to instability. However, simulations indicate that a compromise between operating voltage and gap distance does enable large-amplitude deformation at reasonable electrode voltages.

The magnitude of the transparent electrode potential, in particular, determines the size of localized deformations (e.g., pokes) that can be imposed on the membrane. If the transparent electrode potential is constrained by the stability requirement, then the correspondingly low, opposing electrode array voltages will only enable small, localized membrane deformations.

Large (e.g.,  $>5 \mu\text{m}$ ) localized deformations can be accomplished by low-stress membrane devices made with larger gap distances that are operated at a higher voltage than existing devices. For example, a membrane device with a  $75 \mu\text{m}$  gap distance would generate an  $8.5 \mu\text{m}$  amplitude deformation for  $j = 1$  eigenfunction with electrode array operation at  $110 \text{ V}$ . This same device would exhibit  $2-3 \mu\text{m}$  peak deformation for higher-order eigenmode deformations. As a result, such devices would enable the generation of large, low-spatial-order optical corrections and modest high-spatial-order optical corrections in an adaptive optics system, and such devices would operate at voltages low enough for use with on-chip electronics.

#### Appendix A: Equation of Equilibrium

The equation of equilibrium is found by expressing the total electrostatic plus mechanical energy as an integral, which must be stationary with respect to arbitrary deformations of the membrane.

The electrostatic energy  $U_E$  is found from integrating the volume energy density of the electrostatic field  $E$  on either side of the membrane, i.e., regions I and II defined in Fig. 1. This quantity, expressed as an integral over the volume of regions I and II, is given as

$$U_E = \int \frac{1}{2} \epsilon_0 E_I^2 dV_I + \int \frac{1}{2} \epsilon_0 E_{II}^2 dV_{II}. \quad (\text{A1})$$

For the transparent electrode and array at uniform voltages  $V_T$  and  $V_A$ , respectively, and the membrane

at voltage  $V_M$ , such that the relative voltages are defined as  $V_{TM}$  and  $V_{AM}$ , the electric fields are given by

$$E_I = \frac{V_{TM}}{(d_T + \xi)}, \quad (\text{A2})$$

$$E_{II} = \frac{V_{AM}}{(d_0 - \xi)}. \quad (\text{A3})$$

Below, the membrane will be considered at ground and the absolute voltages are used. Integration over the vertical dimension in Fig. 1 can be carried out to yield an expression in terms of the integral over the membrane surface:

$$U_E = \frac{\epsilon_0}{2} \int \frac{V_A^2}{d_A - \xi} dS + \frac{\epsilon_0}{2} \int \frac{V_T^2}{d_T + \xi} dS. \quad (\text{A4})$$

For the case of an array of discrete electrodes underneath the membrane, each of area  $\Delta s_k$ , the first term on the right-hand side becomes

$$\int \frac{\epsilon_0 V_A^2}{2(d_A - \xi)} dS \Rightarrow \frac{\epsilon_0}{2} \sum_k \frac{V_k^2}{d_A - \xi_k} \Delta s_k, \quad (\text{A5})$$

and the energy is expressed as a sum over the individual electrodes:

$$U_E = \frac{\epsilon_0}{2} \sum_k \frac{V_k^2}{d_A - \xi_k} \Delta s_k + \frac{\epsilon_0}{2} \int \frac{V_T^2}{d_T + \xi} dS. \quad (\text{A6})$$

This case is considered explicitly in Section 4. For the remainder of this appendix, a uniform voltage  $V_A$  will be assumed on all electrodes of the array and the integral expression given in Eq. (A4) will be used.

The mechanical contribution to the energy is found by considering the tension in the membrane, which acts parallel to the surface of the membrane. This tension acts as a restoring force to the membrane that prevents electrostatic-induced snapdown for suitably small deformations. Tension acts to pull the membrane flat, and increasing the tension makes the membrane harder to deform for a given set of voltages applied to the electrodes.

The mechanical contribution to the energy is given by

$$U_T = \frac{1}{2} \int T(\nabla \xi)^2 dS. \quad (\text{A7})$$

This expression ignores the effects of bending stress; prior simulations have demonstrated that bending stress is a small fraction of the material stress (e.g., 10% for low-stress membranes) for deformations that are typical of adaptive optics mirrors.

The total energy  $U = U_E + U_T$  is given by combining Eqs. (A4) and (A7):

$$U = \int \left[ \frac{\epsilon_0}{2} \frac{V_A^2}{d_A - \xi} + \frac{\epsilon_0}{2} \frac{V_T^2}{d_T + \xi} + \frac{1}{2} T(\nabla \xi)^2 \right] dS. \quad (\text{A8})$$

For the membrane to be in static equilibrium, the total energy must be stationary with respect to arbitrary variations  $\delta\xi$  of the membrane shape function. The variation in the total energy is given by

$$\delta U = U(\xi + \delta\xi) - U(\xi), \quad (\text{A9})$$

where

$$U(\xi + \delta\xi) = \int \left[ \frac{\epsilon_0}{2} \frac{V_A^2}{d_A - \xi + \delta\xi} + \frac{\epsilon_0}{2} \frac{V_T^2}{d_T + \xi + \delta\xi} + \frac{1}{2} T \nabla(\xi + \delta\xi) \nabla(\xi + \delta\xi) \right] dS. \quad (\text{A10})$$

The first two terms of the integrand in Eq. (A10) can be expanded as a Taylor series in powers of  $\delta\xi$ , retaining only terms up to  $O(\delta\xi)$ . The third term of the integrand in Eq. (A10) can be multiplied out, also retaining terms up to  $O(\delta\xi)$ , and integrated by parts (the surface term vanishes because  $\delta\xi = 0$  at the membrane boundary). After subtracting the energy  $U(\xi)$ , given by Eq. (A8), these simplifications yield an integral expression for the energy variational:

$$\delta U = \int \left[ -T \nabla^2 \xi - \frac{1}{2} \epsilon_0 \frac{V_A^2}{(d_A - \xi)^2} + \frac{1}{2} \epsilon_0 \frac{V_T^2}{(d_T + \xi)^2} \right] \delta\xi dS. \quad (\text{A11})$$

The condition for equilibrium consists of this integral being an extremum,  $\delta U = 0$ , which for arbitrary variations  $\delta\xi$  requires the quantity in brackets to be zero. This requirement leads to the equation of equilibrium for the membrane:

$$T \nabla^2 \xi = -\frac{\epsilon_0 V_A^2}{2(d_A - \xi)^2} + \frac{\epsilon_0 V_T^2}{2(d_T + \xi)^2}. \quad (\text{A12})$$

Stability of the equilibrium can be analyzed by taking a second variation  $\delta^2 U$  starting from Eq. (A11). This computation, carried out in Subsection 3.B, is complicated by the presence of  $\nabla^2$  in the integrand of Eq. (A11). Expansion of the membrane variation  $\delta\xi$  in eigenfunctions of the  $\nabla^2$  operator allows expression of  $\delta^2 U$  in terms of these eigenfunctions. The resulting energy variational is found as a matrix, whose eigenvalues are used to determine the stability of equilibrium.

## Appendix B: Eigenfunctions of the Membrane

Given a membrane of radius  $a$ , the eigenfunctions  $\zeta_{vn}$  and eigenvalues  $\lambda_{vn}$  satisfy the equation

$$\nabla^2 \zeta_{vn} = -\lambda_{vn}^2 \zeta_{vn}, \quad (\text{B1})$$

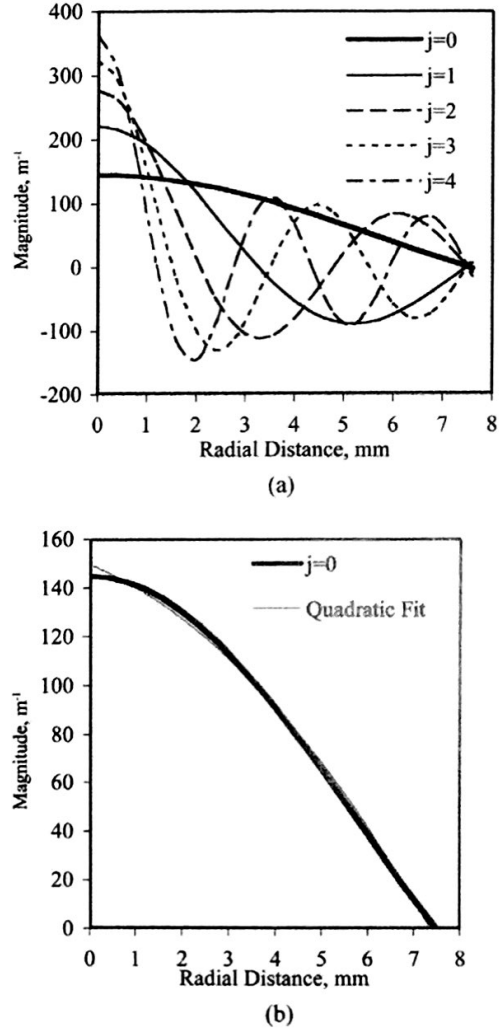


Fig. 6. Representative eigenfunctions for a 7.5 mm radius membrane. Each plot graphs the magnitude of the complex eigenfunction  $\zeta_j(m^{-1})$  versus radial coordinate (mm). (a) First five eigenfunctions, indexed by  $j$  value, as defined in the text. (b) The 0th-order eigenfunction and a quadratic fit. The lowest-order eigenfunction is nearly a parabola.

subject to the boundary condition that the membrane have zero deformation at its periphery, i.e.,  $\zeta_{vn}(r = a) = 0$ . The eigenfunctions are labeled with two integer indices,  $v$  and  $n$ , appropriate for the solution in two dimensions. Equation (B1) can be solved in polar coordinates using separation of variables.<sup>4</sup> The eigenvalues, which are found from the separation constants, are given by

$$\lambda_{vn} = \frac{x_{vn}}{a}, \quad (\text{B2})$$

where  $x_{vn}$  is the  $n$ th zero of Bessel function  $J_v(\rho)$ . Eigenfunctions are given by

$$\zeta_{vn} = \frac{1}{a \sqrt{\pi} |J_{v+1}(x_{vn})|} J_v \left( x_{vn} \frac{\rho}{a} \right) e^{iv\phi}. \quad (\text{B3})$$

These eigenfunctions satisfy the orthonormality condition

$$\int \zeta_{vn} \bar{\zeta}_{v'n'} dS = \delta_{vv'} \delta_{nn'}, \quad (B4)$$

where each  $\delta$  denotes a Kronecker delta,  $\bar{\zeta}_{v'n'}$  is the complex conjugate of  $\zeta_{v'n'}$ , and integration is over the membrane surface  $S$ .

In simulations discussed above, eigenfunctions are labeled by a single index  $j$ , which combines both  $v$  and  $n$  according to  $j = 9v + n - 1$ . Thus the lowest-order modes, corresponding to  $v = 0$ , are composed of

$J_0$  Bessel functions that have  $j$  nodes in the radial direction between the center and the edge of the membrane, and no azimuthal dependence. Representative eigenfunctions are illustrated in Fig. 6.

## References

1. R. Aldrich, "Deformable mirrors wavefront correctors," in *Adaptive Optics Engineering Handbook*, R. Tyson, ed. (Marcel Dekker, 2000), pp. 151–157.
2. G. Vdovin and P. M. Sarro, "Flexible mirror micromachined in silicon," *Appl. Opt.* **34**, 2968–2972 (1995).
3. We are preparing a manuscript to be called, "Fabrication of a membrane mirror with transparent electrode."
4. D. L. Powers, *Boundary Value Problems*, 3rd ed. (Harcourt Brace Jovanovich, 1987), pp. 264–266.